Chemical Science

ROYAL SOCIETY OF CHEMISTRY

EDGE ARTICLE

View Article Online
View Journal | View Issue

Cite this: *Chem. Sci.*, 2021, **12**, 1054

All publication charges for this article have been paid for by the Royal Society of Chemistry

A photo-sensitizable phage for multidrug-resistant *Acinetobacter baumannii* therapy and biofilm ablation†

Bei Ran,[a] Yuyu Yuan,[b] Wenxi Xia,[a] Mingle Li,[a] Qichao Yao,[a] Zuokai Wang,[a] Lili Wang,[b] Xiaoyu Li,[b] Yongping Xu[b] and Xiaojun Peng *[a]

Received 4th September 2020
Accepted 13th November 2020

DOI: 10.1039/d0sc04889e

rsc.li/chemical-science

Antibiotic abuse causes the emergence of bacterial resistance. Photodynamic antibacterial chemotherapy (PACT) has great potential to solve serious bacterial resistance, but it suffers from the inefficient generation of ROS and the lack of bacterial targeting ability. Herein, a unique cationic photosensitizer (NB) and bacteriophage (ABP)-based photodynamic antimicrobial agent (APNB) is developed for precise bacterial eradication and efficient biofilm ablation. Thanks to the structural modification of the NB photosensitizer with a sulfur atom, it displays excellent reactive oxygen species (ROS)-production ability. Moreover, specific binding to pathogenic microorganisms can be provided by bacteriophages. The developed APNB has multiple functions, including bacteria targeting, near-infrared fluorescence imaging and combination therapy (PACT and phage therapy). Both *in vitro* and *in vivo* experiments prove that APNB can efficiently treat *A. baumannii* infection. Particularly, the recovery from *A. baumannii* infection after APNB treatment is faster than that with ampicillin and polymyxin B *in vivo*. Furthermore, the strategy of combining bacteriophages and photosensitizers is employed to eradicate bacterial biofilms for the first time, and it shows the excellent biofilm ablation effect as expected. Thus, APNB has huge potential in fighting against multidrug-resistant bacteria and biofilm ablation in practice.

Introduction

Bacterial infection is recognized as one of the main causes of death and poses a great threat to human health.[1–3] Since penicillin was first discovered to treat bacterial infections, people began to widely use antibiotics for infectious disease therapy. Unfortunately, antibiotic abuse causes the emergence of drug-resistant bacteria, such as vancomycin-resistant *Enterococcus* (VRE), carbapenem-resistant *Enterobacteriaceae* (CRE) and multidrug-resistant *Acinetobacter baumannii* (MRAB).[4,5] Specially, MRAB is a type of Gram-negative bacteria and severe nosocomial infections can be caused by MRAB. In addition, MRAB also exists in the form of biofilms. Bacteria enclosed in biofilms can be 1000 times more resistant to antibiotics.[6,7] The use of polymyxin is regarded as the last chance for treatment of MRAB, but it usually causes significant nephrotoxicity and polymyxin-resistant *Acinetobacter baumannii* is gradually emerging.[8] The emergence and the rapid spread of MRAB make slight injuries difficult to treat, and it is conceivable that there will be no available drugs to use to treat even common infections in the end. Therefore, it is urgent to explore new antibacterial strategies for effectively combating MRAB infections and biofilm ablation.

Photodynamic antimicrobial chemotherapy (PACT) has gained broad attention[9] and the use of many inorganic and metallic nanocomposites is the most researched strategy.[10,11] However such nanomaterials are difficult to degrade *in vivo*, which is the most fatal drawback for their practical application.[12–14] In contrast, organic small molecules have high biosafety owing to easy metabolism *in vivo*, and they hold great promise in PACT.[15–17] However, many of the small molecular photosensitizers (PSs) used in PACT suffer from poor sensitivity due to inefficient generation of ROS and poor selectivity due to the lack of bacterial targeting ability. Thus the aim of this article is to develop a novel PACT agent that possess high selectivity and sensitivity to fight against MRAB and their biofilms.

In this article, we construct a multi-functional antibacterial system based on the ABP phage and Nile blue photosensitizer (NB) for the treatment of multi-drug resistant *A. baumannii* (*A. b*), and the strategy of combining bacteriophages and photosensitizers is also used to eradicate biofilms for the first time (Scheme 1). Nile blue dyes (NB) are cationic photosensitizers and their excellent photodynamic effect has been previously validated.[18–20] Structural modification with a "sulfur atom" can effectively improve the triplet yield, thus improving the sensitivity of PACT. Furthermore, bacteriophages have demonstrated

[a]*State Key Laboratory of Fine Chemicals, Dalian University of Technology, Dalian 116024, China. E-mail: pengxj@dlut.edu.cn*

[b]*School of Bioengineering, Dalian University of Technology, Dalian 116024, China*

† Electronic supplementary information (ESI) available: Experimental methods, optimization of conditions, cell viability, SEM images, and optical microscope photographs of biofilms. See DOI: 10.1039/d0sc04889e

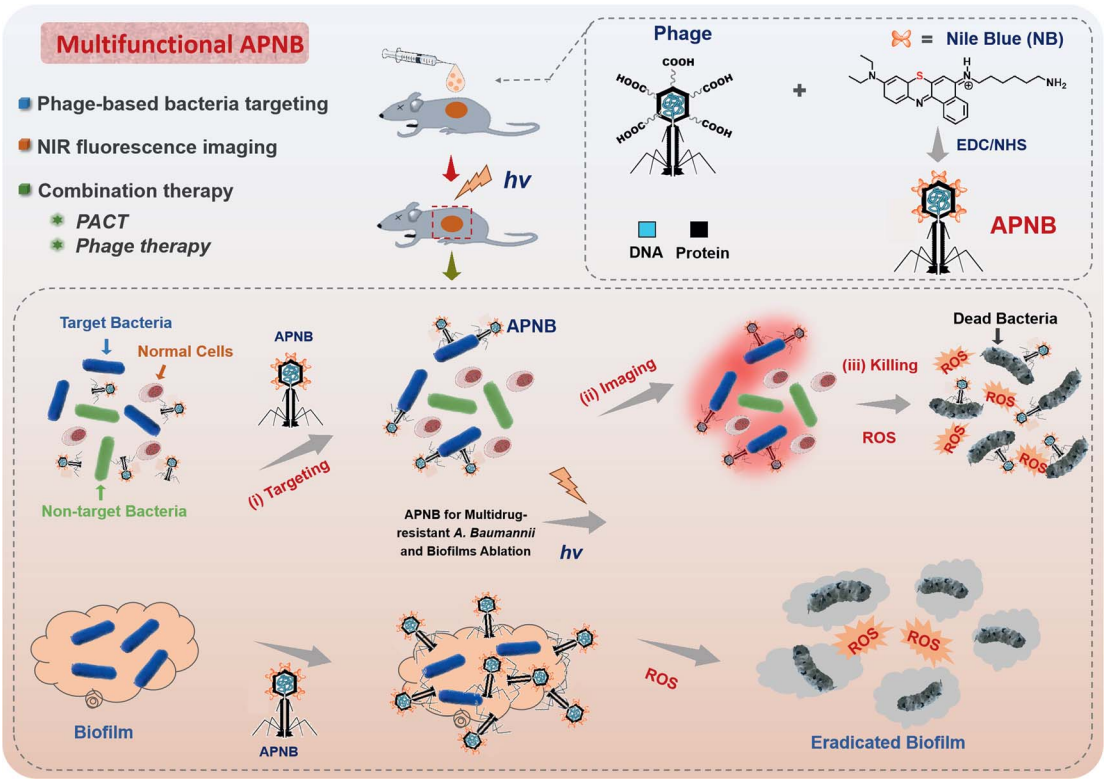

Scheme 1 Schematic of the multi-functional antibacterial system (APNB) based on the ABP phage and Nile blue photosensitizer (NB) for the treatment of multi-drug resistant *Acinetobacter baumannii* and its biofilms. Structural modification of NB with a sulfur atom contributes the high ROS generation ability, and the bacteriophages provide specific binding to pathogenic microorganisms. The developed APNB has multiple functions, including bacteria targeting, near-infrared fluorescence imaging and combination therapy (PACT and phage therapy).

particular specificity to their hosts.[21] Before the discovery and wide use of antibiotics, bacteriophage therapy was an important antibacterial strategy, and it is revived due to the outbreak of antibiotic resistance.[22–24] However, if bacteriophages alone are used in the treatment of bacterial infection, the optimal therapeutic effect often cannot be achieved. Therefore, NB-carried ABP, combining ABP and NB, provides a positive synergistic effect in the killing of pathogens *in vitro* and *in vivo*, and ABP can also enhance the targeting properties of NB photosensitizers as ABP specially targets MRAB. Meanwhile, therapeutic processes can be easily evaluated by the fluorescence of NB, realizing the real-time monitoring of therapeutic efficacy.

Compared with antibiotics, the developed PACT agent (APNB) has the following advantages: (1) it can act on both Gram-positive and Gram-negative bacteria, and is also highly effective against multi-drug resistant bacteria and their biofilms; (2) the particular bacterial targeting properties of APNB owing to the selective binding ability of bacteriophages; (3) resistance is not easy to develop: APNB can bind to the main components of biofilms and eliminate drug resistance caused by biofilms. At the same time, drug internalization is not a prerequisite for PACT to kill bacteria; (4) low toxic and side effects: APNB is injected to the infected sites and light is used to achieve the therapeutic effect, resulting in low damage to normal tissues; (4) multi-target destruction: ROS produced by APNB can destroy proteins, polysaccharides, nucleic acids, lipids and many other substances.

Results and discussion

Synthesis and characterization of the APNB conjugate

The NB-phage bioconjugate (APNB) is first synthesized through the reaction between the carboxyl group in the outside proteins of bacteriophages and the amino group in NB molecules. According to the UV-vis spectra (Fig. 1A), the NB characteristic absorbance peak (668 nm) is observed from the obtained APNB conjugate, suggesting the successful NB loading onto the ABP phage. Furthermore, APNB shows absorption in the therapeutic window (600–900 nm), indicating that APNB has lower phototoxicity to normal tissues and deeper penetration into infected sites. Fig. S1† shows the standard absorbance curves of NB and ABP, respectively. The results show that $Abs_{668\ nm}$ and $Abs_{285\ nm}$ increase linearly with the increase of concentrations of NB and ABP. According to the standard curve method, the concentrations of NB and ABP are calculated to be 0.103 μM and 0.25×10^9 PFU mL^{-1}, respectively. Meanwhile, high near-infrared fluorescence is exhibited after 660 nm excitation (Fig. 1B), indicating that the fluorescence can be maintained after the NB loading onto the ABP phage. The morphology of the ABP phage is observed through transmission electron microscopy (TEM), and the diameter of ABP is about 20 nm (Fig. 1C). In addition, *A. baumannii* is a kind of Gram-negative bacteria, and it has a dense outer membrane, thus usually making PACT have less effect on it. However, lipopolysaccharide molecules in its outer

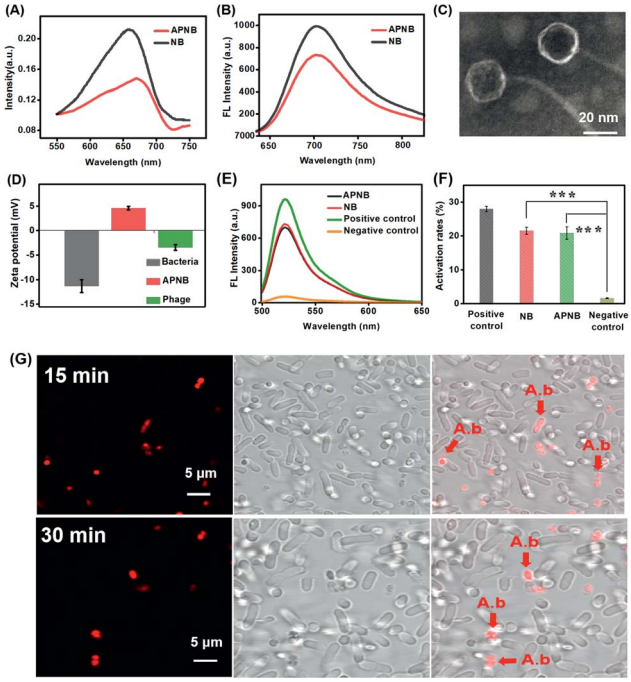

Fig. 1 (A) UV-vis spectra and (B) fluorescence spectra of NB and APNB. (C) TEM image of the ABP phage (scale bar = 20 nm). (D) Zeta potentials of *A. baumanni*, the ABP phage and APNB in water. (E) Relative fluorescence intensity and (F) activation rates of 2′,7′-dichlorofluorescein (DCFH) with addition of APNB, NB, the positive control and the negative control upon exposure of 660 nm light (20 mW cm^{-2}). ***$P < 0.001$. (G) Targeted bacterial imaging of APNB by fluorescence imaging of *A. baumanni* and *P. aeruginosa* co-incubated with APNB for 15 min and 30 min. Arrows indicate *A. baumannii* with staining by APNB (scale bar = 5 μm). [APNB] = 0.5 μM. λ_{ex} = 660 nm for APNB.

membrane are negatively charged, and thus this kind of cationic photosensitizer (APNB) can easily bind and penetrate into *A. baumannii* through electrostatic adsorption, and shows the potential antibacterial activity for *A. baumannii* (Fig. 1D).

Detection of ROS

The ability of ROS production is a key factor that needs to be considered for an outstanding PACT agent.[25,26] Thus we use 2′,7′-dichlorofluorescein (DCFH) as a probe to explore the ROS generation ability of APNB, and utilize UV-vis spectroscopy to measure the generation rate of ROS. A positive control and negative control are used as the reference. As shown in Fig. 1E and F, after light exposure, APNB can efficiently sensitize surrounding oxygen to produce ROS, and the ROS generation of APNB is nearly equal to that of NB. The results show that APNB can rapidly generate ROS and has the potential to act as an ideal PACT agent for *A. baumanni* killing.

Specific targeting imaging for *A. baumanni* by APNB

It has been demonstrated that bacteriophages have specific targeting ability to their hosts.[27,28] Compared with the antibody-based targeting strategy, they have the following advantages: (1) the large surface area enables more photosensitizer delivery; (2) the bacteria targeting ability can be adjusted as needed. Therefore, based on the particular recognition of the ABP phage, we investigate the bacteria targeting ability of APNB through confocal laser scanning microscope (CLSM) imaging of *A. baumanni* and *P. aeruginosa* co-incubated with APNB for 15 min and 30 min. As shown in Fig. S2,† a bright fluorescence signal is observed in *A. baumannii* after incubating with APNB for 30 min and 660 nm light irradiation for 15 min, while there is almost no red fluorescence from APNB in *P. aeruginosa* under light irradiation. Futhermore, the real-time monitoring of bacteria targeting in mixed microbes using the APNB probe is examined. As shown in Fig. 1G, when the mixed bacteria including host bacteria (*A. baumannii*) and *P. aeruginosa* are incubated with APNB, only *A. baumannii* can be specifically stained under light irradiation, and *P. aeruginosa cannot* be stained by APNB absolutely. The arrows indicate the stained *A. baumannii* by APNB. The results confirm the specific targeting ability of APNB and its great promise in precise antibacterial therapy.

Evaluation of *in vitro* antibacterial activity

The ABP phage not only has the function of bacteria targeting, but also has an antibacterial effect. Therefore, the constructed APNB system has dual antibacterial effects, including photodynamic therapy and phage therapy. In order to test the synergistic photodynamic killing effect of APNB *in vitro*, *A. baumannii* in the log phase is treated with ABP, NB and APNB respectively. Firstly, we optimize therapy conditions including the time of APNB incubation and light exposure through evaluating the survival rate of *A. baumannii*. As shown in Fig. S3,† the survival rate of *A. baumannii* decreases from 32.3% to 5.6% along with different incubation times (10, 20 and 30 min) and a fixed light exposure time (15 min), and thus 30 min is chosen as the optimal APNB incubation time. Then, we fix 30 min of APNB incubation and excite the bacterial suspensions by using 660 nm light (20 mW cm^{-2}) for 5, 10, and 15 min, respectively. Nearly 94% of *A. baumannii* can be killed after 15 min of light exposure (Fig. S4†), and 15 min is chosen as the optimal irradiation time. Therefore, the 30 minutes of incubation and 15 minutes of light exposure are employed in the following antibacterial experiments.

To confirm the antibacterial effect of PACT with APNB, a live/dead bacterial viability kit is first used to stain the treated bacteria by confocal laser scanning microscope (CLSM) imaging. The live bacterial cells show as green and the dead bacterial cells show as red because of the intact and damaged membrane. As shown in Fig. 2C and 2D, the free NB group and control group exhibit a large amount of green fluorescence, indicating that all bacteria are alive, while almost all bacteria in the APNB-group show red fluorescence because of the effective killing with light irradiation by APNB (Fig. 2A). In the ABP-treated group, ABP also shows moderate toxicity toward *A. baumannii* because of the intrinsic antibacterial activity of the ABP phage (Fig. 2B).

One of the other key issues for PACT application is the biosafety of the PACT agent. In terms of this issue, we study the

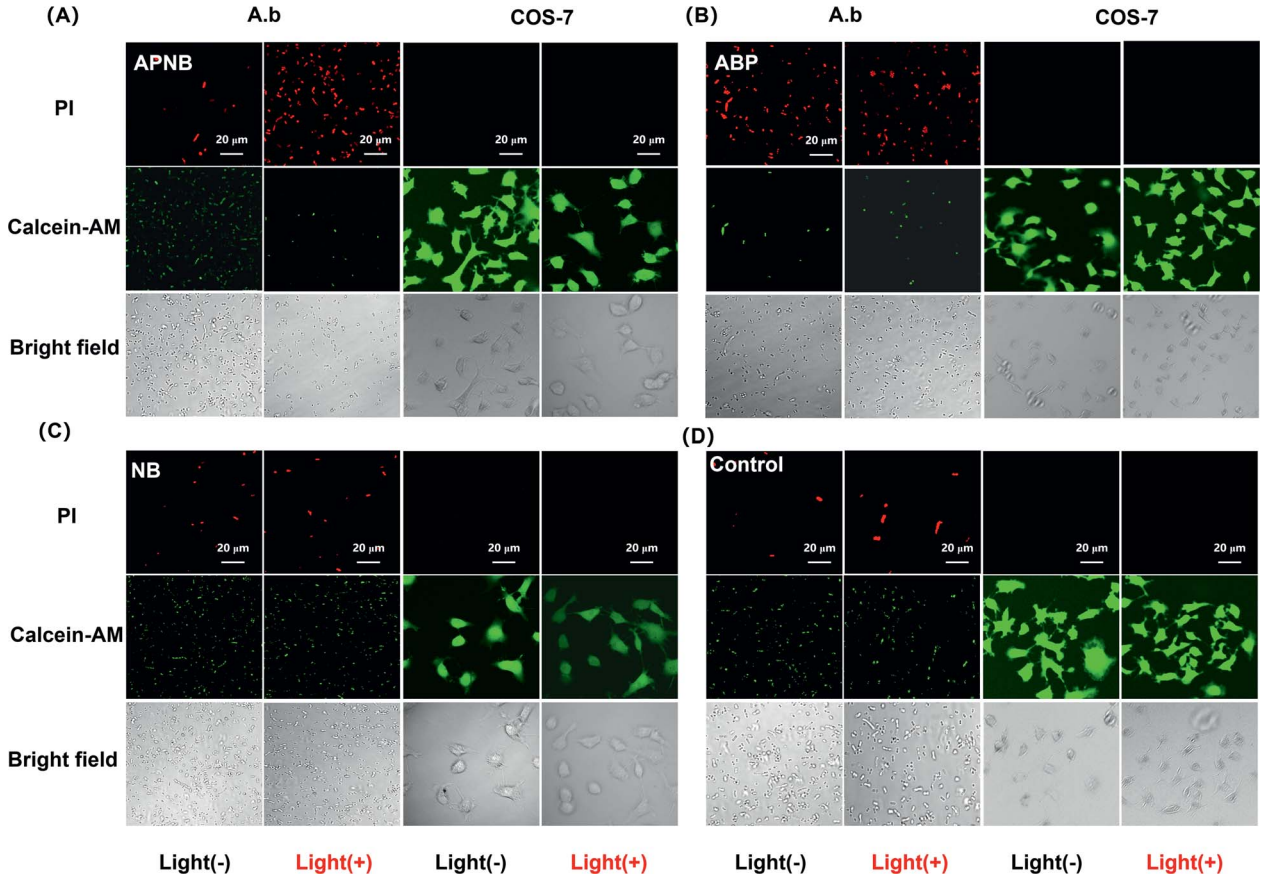

Fig. 2 Live/dead bacterial viability test by confocal laser scanning microscope (CLSM) imaging. (A) Confocal images of APNB-treated bacteria and COS-7 cells post live/dead staining (scale bar = 20 μm). (B) Confocal images of ABP-treated bacteria and COS-7 cells post live/dead staining (scale bar = 20 μm). (C) Confocal images of NB-treated bacteria and COS-7 cells post live/dead staining (scale bar = 20 μm). (D) Confocal images of control group post live/dead staining (scale bar = 20 μm). The PACT treatment is conducted under 660 nm light irradiation (20 mW cm^{-2}) for 15 min. [APNB] = [NB] = 0.5 μM. [Calcein-AM] = 5 μM. [PI] = 5 μM. λ_{ex} = 490 nm for Calcein-AM, and λ_{ex} = 530 nm for PI.

binding ability of APNB towards mammalian cells *in vitro*, and COS-7 cells are selected as the models. According to the live/dead staining results, all the COS-7 cells in the APNB-group display bright green fluorescence, demonstrating that APNB shows almost no killing effect against COS-7 cells (Fig. 2A), furthermore confirming its perfect selectivity and bio-safety towards mammalian cells.

To eliminate bacteria, APNB must be close to and penetrate into the outer surfaces of bacterial cells, which allows the generation of a large amount of ROS and the destruction of proteins, polysaccharides, nucleic acids, lipids and many other substances in bacterial cells.[29–31]

Hence, the intracellular ROS levels are next evaluated using confocal laser scanning microscope (CLSM) imaging. We use DCFH staining to study intracellular ROS production in APNB-treated *A. baumannii*. As shown in Fig. 3, there is almost no green fluorescence from DCF in *A. baumannii* in the absence of APNB and slight green fluorescence in the presence of NB. In contrast, the distinct green fluorescence from DCF is observed in *A. baumannii* when treated with APNB under light irradiation. Meanwhile, the fluorescence intensity increases as the concentration of APNB increases from 0.25 μM to 0.5 μM (Fig. S5†), suggesting that much more ROS can be produced because APNB can specifically bind to *A. baumannii*. When compared to COS-7 cells, APNB shows relatively weak binding

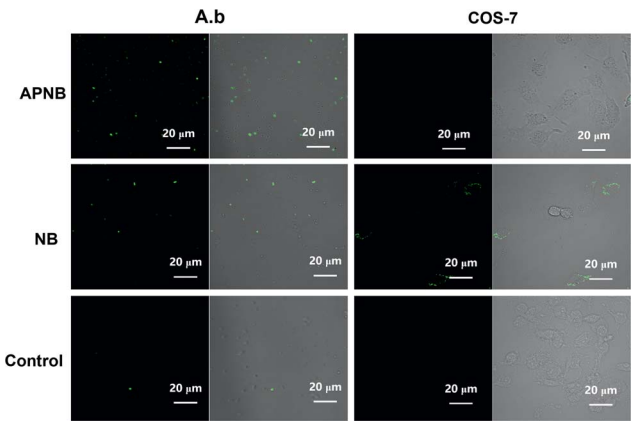

Fig. 3 Intracellular detection of ROS production in APNB-treated *A. baumannii* and COS-7 cells using confocal laser scanning microscope (CLSM) imaging (scale bar = 20 μm). [APNB] = [NB] = 0.5 μM. [DCFH] = 10 μM. λ_{ex} = 488 nm for DCH.

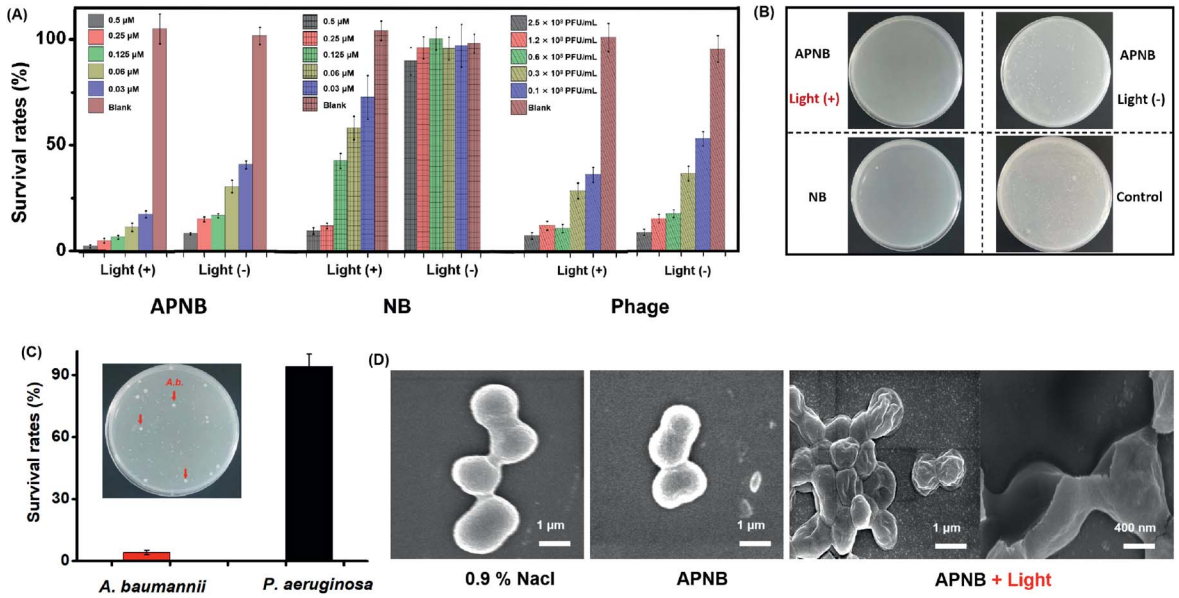

Fig. 4 Antibacterial evaluation of APNB based PACT *in vitro*. (A) Survival rates of bacteria and (B) viable bacteria remained in the culture after different treatments using the CFU counting method. (C) *A. baumannii* and *P. aeruginosa* are incubated together with APNB. The arrows indicate *A. baumannii* identified *via* the colony morphology. (D) SEM images of *A. baumannii* before and after being treated with APNB (scale bar = 1 μm).

affinity with COS-7 cells because no fluorescence is observed through DCFH staining. In contrast, when treated with NB, light fluorescence in COS-7 cells is observed, and the fluorescence intensity increases as the concentration of NB increases from 0.25 μM to 0.5 μM, demonstrating the better selectivity of APNB (Fig. S6†).

Based on the above results, we study the *in vitro* antibacterial activity of APNB against *A. baumannii* utilizing the colony-forming units (CFU) counting method under 660 nm light irradiation (20 mW cm^{-2}) for 15 min. As shown in Fig. 4A and B, both the NB-treated group and phage-treated group show moderate antibacterial activity with light exposure. In the APNB-treated group, APNB also shows moderate toxicity toward *A. baumannii* without light exposure probably because of the intrinsic antibacterial activity of the phage. However upon 660 nm light irradiation and a low dose of APNB (0.03 μM), the growth rate of *A. baumannii* could be inhibited effectively as low as 17.63%, which was far above that of the NB or phage-treated group. It indicates that the light-excited APNB can damage the bacterial cells and enhance bacteria killing.

The targeted killing of bacteria is another key factor for evaluation of the antibacterial effect. This capability of APNB is verified in mixed systems by culturing host bacteria (*A. baumannii*) with non-host bacteria (*P. aeruginosa*), respectively. As shown in Fig. 4C, in the presence of light irradiation, *A. baumannii* are killed effectively and few colonies formed with APNB treatment. However the colony quantity of *P. aeruginosa* is nearly uninfluenced, which agrees with the above result of targeting imaging for *A. baumanni* by APNB.

To furthermore explore whether APNB could disrupt the integrity of the bacterial cell membrane, a scanning electron microscope (SEM) is used to study the microscopic structure of *A. baumannii* before and after PACT. As shown in Fig. 4D, the untreated *A. baumannii* displays intact cell walls with a smooth surface. By contrast, after incubation with APNB at a concentration of 0.5 μM and applying light illumination for 15 min, the cell walls are wrinkled and the cellular structures, particularly the outer membrane, are wholly ruptured and collapsed, indicating that the *A. baumannii* have been killed owing to the leakage of intracellular contents (Fig. S8†). The morphological structures of bacteria observed by SEM further confirm that the light-excited APNB could greatly damage the cell membrane and has great potential to be used for *A. baumannii* treatment *in vivo*.

Cytotoxicity assay

For *in vivo* applications, cell viability is an important characteristic that needs to be checked. The MTT assay is employed to investigate the cytotoxicity of APNB. As shown in Fig. S7,† after incubation with APNB for 24 h without light irradiation, the cell viability is over 90% at concentrations lower than 0.5 μM, confirming the low dark cytotoxicity of APNB. When the cells are treated with APNB for 24 h followed by 660 nm light (20 mW cm^{-2}) irradiation for 15 min, the cell viability exceeds 83% at a concentration of 0.5 μM. When the concentration further decreases, the cell viability increases to more than 90%. Cytotoxicity experiments verify that APNB shows excellent biocompatibility, which is much better than that of NB.

Bacterial biofilm ablation and inhibition effects *in vitro*

Besides the free form, MRAB also exists in the form of biofilms.[32–34] In clinics, a large number of implantable medical device-caused bacterial infections are related to MRAB biofilms.[35,36] Once the biofilms are formed on the surface of implantable devices, they are difficult to eradicate due to the protection of the polymeric matrix in biofilms. What's worse,

antibiotics and other kinds of drugs can be prevented from penetrating into bacteria by the polymeric matrix in biofilms. The bacteria enclosed in the biofilms can be 1000 times more resistant to antibiotics.[37,38] Thus, it takes a lot of effort for biofilm removal, such as washing with acidic compounds or strong oxidizing agents and high pressure water jet cleaning devices, but those suffer from the high costs and need of high energy devices.[39,40]

Encouraged by the highly efficient antibacterial ability of light-excited APNB, the combination of PACT and the phage is also expected to effectively eradicate existing biofilms and inhibit biofilm formation. The capability of APNB to ablate existing biofilms and prevent the formation of bacterial biofilms is investigated through a crystal violet (CV) staining assay. As shown in Fig. 5A, the APNB-treated group exhibits excellent ablation effects on the biofilms with light exposure, and the biofilm ablation rate is 89.3% when the concentration of APNB is up to 0.5 μM, and APNB could efficiently ablate the bacterial biofilms at a low concentration (0.25 μM). The photographs (Fig. 5B) and optical microscope photographs (Fig. 5C) of the remaining biofilms after the different treatments also confirm the efficient biofilm ablation effect. Besides, the bacterial biofilms are obviously ablated in a concentration-dependent manner of APNB (Fig. S9†). Surprisingly, the NB-treated group shows remarkable ability of biofilm ablation as well. The biofilm ablation rate is 74.8% when the concentration of NB is up to 0.5 μM, and it could also efficiently ablate the bacterial biofilms at a low concentration (0.25 μM) (Fig. 5A).

Apart from the ability to effectively eradicate existing biofilms, APNB is also able to efficiently inhibit biofilm formation. Fig. 5D and S10† show the CV staining results for the formed biofilms after treatment with APNB without or with light irradiation. Limited inhibition effects are observed after treatment with 0.9% NaCl. After treatment with the phage, NB, and APNB with NIR light, the inhibition effect is significantly enhanced, and APNB exhibits the highest inhibition effect. CFU counting assay also confirms the inhibition of the biofilm formation by APNB (Fig. 5E).

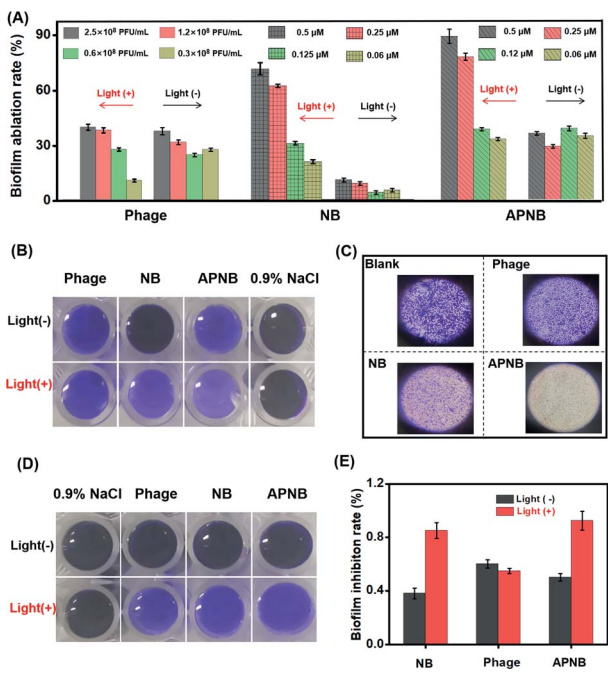

Fig. 5 (A) *In vitro A. baumannii* biofilm eradication by APNB without or with light irradiation (15 min at 20 mW cm^{-2}); phage and NB served as the controls. (B) The Photographs and (C) optical microscope photographs of the remaining biofilms after the different treatments. (D) Photographs of *in vitro* inhibition of biofilm formation by the phage, NB and APNB without or with NIR light irradiation (15 min at 20 mW cm^{-2}); the phage and NB served as the controls. (E) Biofilm inhibition rate of APNB by CFU counting.

Evaluation of the *in vivo* antibacterial effect

Encouraged by the excellent *in vitro* antibacterial effect, the *in vivo* antibacterial effect of APNB is explored. 6–8 weeks female BALB/c mice, with 1×10^8 CFU *A. baumannii* triggered skin infection, are used as the models to evaluate the *in vivo* antibacterial effect of APNB. The infected mice are randomly assigned to four groups for the following different treatments: 0.9% NaCl, ampicillin, polymyxin B, and APNB. The APNB is the PACT group, while the ampicillin and polymyxin B are positive control groups and 0.9% NaCl is the negative control group. Fig. 6A shows the experimental procedure of the *in vivo* antibacterial evaluation; at day 1 and day 2 post injection of *A. baumannii*, the different treatments are conducted. As shown in Fig. 6B, the infected mice that are treated with APNB and exposed to 660 nm light can recover more rapidly compared to the control groups at the 4th day, including the untreated control group, NB group and APNB without light exposure group. As shown in Fig. 6C, the mice in AP the NB-treated group almost recover at the 7th day, and the recovery rate is noticeably faster than that of ampicillin (AMP) and polymyxin B (PB). Meanwhile, mice with the treatment of 0.9% NaCl (control), cannot fully recover even after 10 days, demonstrating that APNB can effectively suppress the bacterial infection. At day 3 post injection of *A. baumannii*, we collect the skin tissues from

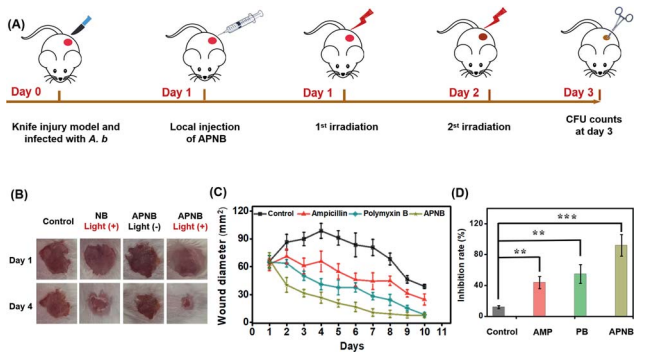

Fig. 6 The antibacterial ability *in vivo*. (A) Experimental procedure of the *in vivo* antibacterial evaluation; the different treatments are conducted at day 1 and day 2 post injection of *A. baumannii*. (B) Photographs and (C) the sizes of the infected areas. (D) the number of bacterial colony-forming units counting from the infected wounds at day 3 post injection of *A. baumannii*. $^{**}P < 0.01$ and $^{***}P < 0.001$.

the infected wounds for CFU counting. As shown in Fig. 6D, *A. baumannii* could be effectively killed and there is a negligible amount of *A. baumannii* in the APNB group under light irradiation, whereas other groups including positive control groups (ampicillin and polymyxin B) and the negative control group (0.9% NaCl) are still infected by *A. baumannii*. To further investigate the bio-safety of APNB, the body weights of the treated mice are measured, and they show a similar trend regardless of the treatment (Fig. S11†). The above results demonstrate that APNB can effectively kill *A. baumannii* and can act as an effective PACT agent to treat *A. baumannii* infection *in vivo*.

Conclusions

In summary, the ABP phage with photosensitizer (NB) conjugation (APNB) is fabricated in this work as a new generation photodynamic antibacterial agent for highly efficient antibacterial treatment and the ablation of biofilms. Thanks to the structural modification of the NB photosensitizer with a sulfur atom, it shows a high ROS generation ability. Moreover, the bacteriophages provide specific binding to pathogenic microorganisms. Compared with free NB, APNB shows greatly enhanced *in vitro* PACT-induced antibacterial efficacy towards *A. baumannii* owing to the ability of phage-based bacterial targeting. Experiments with mouse *A. baumannii* infection further confirm the excellent *in vivo* anti-infection performances of APNB, and the recovery after treatment with our APNB is faster than that with ampicillin and polymyxin B. Furthermore, the strategy of combining bacteriophages and photosensitizers is employed to eradicate bacterial biofilms for the first time, and it shows the excellent biofilm ablation effect *in vitro*. In summary, the above results clearly show that APNB is a highly efficient and multifunctional antibacterial agent, and it has great potential in combating MRAB infections and biofilm ablation.

Conflicts of interest

There are no conflicts to declare.

Acknowledgements

This work was supported by the National Natural Science Foundation of China (project 21421005), National Natural Science Foundation of China (project 22008025), and NSFC-Liaoning United Fund U1608222 and U1908202.

Notes and references

1 M. Baym, L. K. Stone and R. Kishony, *Science*, 2016, **351**, aad3292.
2 J. Besser, H. A. Carleton, P. Gerner-Smidt, R. L. Lindsey and E. Trees, *Clin. Microbiol. Infect.*, 2018, **24**, 335–341.
3 B. R. Levin, F. Baquero, P. Ankomah and I. C. McCall, *Trends Microbiol.*, 2017, **25**, 878–892.
4 W. Chin, G. Zhong, Q. Pu, C. Yang, W. Lou, P. F. De Sessions, B. Periaswamy, A. Lee, Z. C. Liang, X. Ding, S. Gao, C. W. Chu, S. Bianco, C. Bao, Y. W. Tong, W. Fan, M. Wu, J. L. Hedrick and Y. Y. Yang, *Nat. Commun.*, 2018, **9**, 914–917.
5 D. Wong, T. B. Nielsen, R. A. Bonomo, P. Pantapalangkoor, B. Luna and B. Spellberg, *Clin. Microbiol. Infect.*, 2017, **30**, 409–447.
6 H. Koo, R. N. Allan, R. P. Howlin, P. Stoodley and L. Hall-Stoodley, *Nat. Rev. Microbiol.*, 2017, **15**, 740–755.
7 C. R. Arciola, D. Campoccia and L. Montanaro, *Nat. Rev. Microbiol.*, 2018, **16**, 397–409.
8 L. Poirel, A. Jayol and P. Nordmann, *Clin. Microbiol. Rev.*, 2017, **30**, 557–596.
9 M. Wainwright, T. Maisch, S. Nonell, K. Plaetzer, A. Almeida, G. P. Tegos and M. R. Hamblin, *Lancet Infect. Dis.*, 2017, **17**, e49–e55.
10 W. Chen, J. Ouyang, H. Liu, M. Chen, K. Zeng, J. Sheng, Z. Liu, Y. Han, L. Wang, J. Li, L. Deng, Y.-N. Liu and S. Guo, *Adv. Mater.*, 2017, **29**, 1603864.
11 W. Liu, Y. Zhang, W. You, J. Su, S. Yu, T. Dai, Y. Huang, X. Chen, X. Song and Z. Chen, *Nanoscale*, 2020, **12**, 13948–13957.
12 C. Wang, Y. Xiao, W. Zhu, J. Chu, J. Xu, H. Zhao, F. Shen, R. Peng and Z. Liu, *Small*, 2020, **16**, 2000589.
13 K. Turcheniuk, V. Turcheniuk, C.-H. Hage, T. Dumych, R. Bilyy, J. Bouckaert, L. Héliot, V. Zaitsev, R. Boukherroub and S. Szunerits, *Chem. Commun.*, 2015, **51**, 16365–16368.
14 S. Gao, X. Yan, G. Xie, M. Zhu, X. Ju, P. J. Stang, Y. Tian and Z. Niu, *Proc. Natl. Acad. Sci. U.S.A.*, 2019, **116**, 23437–23443.
15 J. Zhuang, H. Yang, Y. Li, B. Wang, N. Li and N. Zhao, *Chem. Commun.*, 2020, **56**, 2630–2633.
16 J. S. Ni, T. Min, Y. Li, M. Zha, P. Zhang, C. L. Ho and K. Li, *Angew. Chem., Int. Ed.*, 2020, **59**, 10179–10185.
17 E. Lee, X. Li, J. Oh, N. Kwon, G. Kim, D. Kim and J. Yoon, *Chem. Sci.*, 2020, **11**, 5735–5739.
18 M. Li, J. Xia, R. Tian, J. Wang, J. Fan, J. Du, S. Long, X. Song, J. W. Foley and X. Peng, *J. Am. Chem. Soc.*, 2018, **140**, 14851–14859.
19 M. Xiao, W. Sun, J. Fan, J. Cao, Y. Li, K. Shao, M. Li, X. Li, Y. Kang, W. Zhang, S. Long, J. Du and X. Peng, *Adv. Funct. Mater.*, 2018, **28**, 1805128.
20 M. Li, Y. Shao, J. H. Kim, Z. Pu, X. Zhao, H. Huang, T. Xiong, Y. Kang, G. Li, K. Shao, J. Fan, J. W. Foley, J. S. Kim and X. Peng, *J. Am. Chem. Soc.*, 2020, **142**, 5380–5388.
21 X. He, Y. Yang, Y. Guo, S. Lu, Y. Du, J.-J. Li, X. Zhang, N. L. C. Leung, Z. Zhao, G. Niu, S. Yang, Z. Weng, R. T. K. Kwok, J. W. Y. Lam, G. Xie and B. Z. Tang, *J. Am. Chem. Soc.*, 2020, **142**, 3959–3969.
22 R. Agarwal, C. T. Johnson, B. R. Imhoff, R. M. Donlan, N. A. McCarty and A. J. García, *Nat. Biomed. Eng.*, 2018, **2**, 841–849.
23 K. Yehl, S. Lemire, A. C. Yang, H. Ando, M. Mimee, M. D. T. Torres, C. de la Fuente-Nunez and T. K. Lu, *Cell*, 2019, **179**, 459–469.
24 T. K. Lu and J. J. Collins, *Proc. Natl. Acad. Sci. U.S.A.*, 2007, **104**, 11197–11202.
25 L. Wang, Y. Li, L. Zhao, Z. Qi, J. Gou, S. Zhang and J. Z. Zhang, *Nanoscale*, 2020, **12**, 19516–19535.

26 Z. Zheng, H. Liu, S. Zhai, H. Zhang, G. Shan, R. T. K. Kwok, C. Ma, H. H. Y. Sung, I. D. Williams, J. W. Y. Lam, K. S. Wong, X. Hu and B. Z. Tang, *Chem. Sci.*, 2020, **11**, 2494–2503.
27 K. S Sunderland, M. Yang and C. Mao, *J. Am. Chem. Soc.*, 2017, **56**, 1964–1992.
28 I. Yosef, M. Manor, R. Kiro and U. Qimron, *Proc. Natl. Acad. Sci. U.S.A.*, 2015, **112**, 7267–7272.
29 Y. Wang, Y. Yang, Y. Shi, H. Song and C. Yu, *Adv. Mater.*, 2020, **32**, 1904106.
30 N. A. Smith, P. Zhang, S. E. Greenough, M. D. Horbury, G. J. Clarkson, D. McFeely, A. Habtemariam, L. Salassa, V. G. Stavros, C. G. Dowson and P. J. Sadler, *Chem. Sci.*, 2017, **8**, 395–404.
31 M. Chen, Z. Long, R. Dong, L. Wang, J. Zhang, S. Li, X. Zhao, X. Hou, H. Shao and X. Jiang, *Small*, 2020, **16**, 1906240.
32 C. Wang, P. Chen, Y. Qiao, Y. Kang, C. Yan, Z. Yu, J. Wang, X. He and H. Wu, *Theranostics*, 2020, **10**, 4795–4808.
33 Q. Deng, P. Sun, L. Zhang, Z. Liu, H. Wang, J. Ren and X. Qu, *Adv. Funct. Mater.*, 2019, **29**, 1903018.
34 Z. Yuan, C. Lin, Y. He, B. Tao, M. Chen, J. Zhang, P. Liu and K. Cai, *ACS Nano*, 2020, **14**, 3546–3562.
35 H. Wang, D. E. Christiansen, S. Mehraeen and G. Cheng, *Chem. Sci.*, 2020, **11**, 4709–4721.
36 J. Guo, Y. Liu, Y. Chen, J. Li and H. Ju, *Chem. Sci.*, 2018, **9**, 5906–5911.
37 M. Ucuncu, B. Mills, S. Duncan, M. Staderini, K. Dhaliwal and M. Bradley, *Chem. Commun.*, 2020, **56**, 3757–3760.
38 Y. Zhao, C. Yu, Y. Yu, X. Wei, X. Duan, X. Dai and X. Zhang, *ACS Appl. Mater. Interfaces*, 2019, **11**, 39648–39661.
39 P. Li, S. Liu, W. Cao, G. Zhang, X. Yang, X. Gong and X. Xing, *Chem. Commun.*, 2020, **56**, 2316–2319.
40 Z. Yuan, B. Tao, Y. He, C. Mu, G. Liu, J. Zhang, Q. Liao, P. Liu and K. Cai, *Biomaterials*, 2019, **223**, 119479.